Stokesian dynamics of close particles

Maria L. Ekiel-Jeżewska[1], Tomasz Gubiec[1,2] and P. Szymczak[3]

[1] *Institute of Fundamental Technological Research, Polish Academy of Sciences, Świętokrzyska 21, 00-049 Warsaw, Poland*

[2] *Institute of Experimental Physics, Warsaw University, Hoża 69, 00-681 Warsaw, Poland and*

[3] *Institute of Theoretical Physics, Warsaw University, Hoża 69, 00-681 Warsaw, Poland*

(Dated: 22.12.2007)

Stokesian dynamics simulations of close particles are reported, taking into account lubrication forces and many-body hydrodynamic interactions between spheres. A periodic trajectory of three particles maintaining a constant proximity to each other has been found and analyzed. This solution is used as a benchmark to study the accuracy and stability of various numerical integration schemes. In particular, different methods of preventing unphysical overlaps of the particles are considered and potential artifacts discussed.

I. INTRODUCTION

The paper is focused on hydrodynamic interactions between very close solid spheres moving in a viscous fluid at the low Reynolds number [1, 2]. Hydrodynamic interactions influence significantly statistical properties of suspensions, and therefore a lot of work has been done to analyze them theoretically [1] and to construct numerical codes suited for efficient and accurate computations, such as lattice Boltzmann [3] and Stokesian dynamics [4, 5]. For dense systems, interaction between very close particle surfaces is essential. As the spheres approach each other at a very small distance it becomes increasingly difficult to squeeze out the thin lubrication layer of fluid from in between them. The hydrodynamic lubrication forces associated with this motion [6] prevent the particles from touching each other. Lubrication of very close solid surfaces is hard to tackle numerically. In particular, due to the numerical errors in the finite-difference schemes, there is often a possibility of an unphysical overlap of the particles, which needs to be carefully avoided in the simulations. Several methods for assisting with this problem have been devised [7–12]. However, they

introduce numerical artifacts, which may significantly influence the dynamics of the particles at short distances [10, 12, 13]. In this paper, we investigate these effects.

In a number of systems, motion of several spheres was detected experimentally or evaluated by the Stokesian dynamics, and some very close configurations of the spheres were observed, with the distance between the sphere surfaces smaller than 10^{-2} radii [14–16]. A lot of examples of 'scattering processes' is known, during which very small gaps between the particle surfaces are reached and then particles again separate – for example, a sphere falling under gravity onto the other one held fixed or moving slower below [14, 15]. The question arises if there exist stable systems of a different nature – with at least three spheres staying very close to each other for a long time.

In this paper, Stokesian dynamics method based on irreducible multipole representation [5, 17] is used to find and investigate a family of such "benchmark clusters", made of a small number of close particles, which settle under gravity. We study a periodic trajectory of three spheres, during which all of them remain in a close proximity of each other. Such a trajectory is ideally suited for testing various numerical schemes, since - as it turns out - even small numerical errors or artifacts may result in significant changes of the observed period of motion. Moreover, the oscillations of very close sedimenting triplets are also of fundamental physical importance.

In Sec. II, theoretical foundations of the Stokesian dynamics – the multipole algorithm [5] and the numerical procedure [17] – are outlined. Sec. III contains a brief review of methods used to integrate numerically the dynamics of very close spheres. In Sec. IV, the periodic motion of three very close spheres is analyzed. In Sec. V, this system is used to test selected numerical procedures, with the conclusions presented in Sec. VI.

II. DYNAMICS

Consider a system made of identical solid spheres of diameters d, which settle under gravitational forces $\mathbf{f}$ in a fluid of viscosity η. The spheres are close to each other, but their surfaces do not touch. The Reynolds number of the generated flow is much smaller than unity. Therefore the fluid velocity $\mathbf{u}$ and pressure p satisfy the Stokes equations,

$$\eta \boldsymbol{\nabla}^2 \mathbf{u} - \boldsymbol{\nabla} p = \mathbf{0}, \tag{1}$$

$$\boldsymbol{\nabla} \cdot \mathbf{u} = 0. \tag{2}$$

The no-slip boundary conditions are satisfied at the sphere surfaces. Positions of the sphere centers $\mathbf{r}_i$ evolve according to the following Stokesian dynamics equations,

$$\frac{d\mathbf{r}_i}{dt} = \mathbf{v}_i(\mathbf{r}_1, \mathbf{r}_2, \ldots, \mathbf{r}_N), \qquad i = 1, 2, ..., N, \tag{3}$$

$$\mathbf{v}_i = \left[\sum_{k=1}^{N} \boldsymbol{\mu}_{ik}\right] \cdot \mathbf{f}, \tag{4}$$

where $\boldsymbol{\mu}_{ik}(\mathbf{r}_1, \mathbf{r}_2, \ldots, \mathbf{r}_N)$ are the N-particle translational-translational mobility matrices [1], [18], evaluated numerically by the multipole expansion of the Stokes equations. The algorithm from Ref. [5] and its precise numerical FORTRAN implementation described in Ref. [17] have been used with the multipole order $L = 4$. To describe accurately dynamics of close spheres, lubrication correction has been applied according to the procedure taken from Ref. [17]. For rigid-body motions, the relative accuracy of the mobility matrix is typically of the order of 0.01% for $L = 4$, see Ref. [5].

It is convenient to use $3N$-dimensional vectors of the particle positions & velocities, and the forces exerted by them on the fluid, $\mathbf{X} = (\mathbf{r}_1, \mathbf{r}_2, \ldots, \mathbf{r}_N)$, $\mathbf{V} = (\mathbf{v}_1, \mathbf{v}_2, \ldots, \mathbf{v}_N)$, and $\mathbf{F} = (\mathbf{f}, \mathbf{f}, \ldots, \mathbf{f})$, respectively. In this notation, the system of Eqs. (3)-(4) reads

$$\frac{d\mathbf{X}}{dt} = \mathbf{V}(\mathbf{X}), \tag{5}$$

$$\mathbf{V} = \boldsymbol{\mu} \cdot \mathbf{F}. \tag{6}$$

The dimensionless variables are obtained by dividing positions by the sphere diameter d and time by twice the Stokes time,

$$\tau_s = 3\pi\eta d^2/f, \tag{7}$$

with $f = |\mathbf{f}|$. Therefore velocities are normalized by the Stokes velocity $v_s = f/(3\pi\eta d)$. From now on, $\mathbf{r}_i$, $\mathbf{v}_i$ and t will denote the dimensionless quantities.

III. NUMERICAL INTEGRATION

In general, due to lubrication forces, the normal relative motion of the particle pair is strongly hindered as the dimensionless gap between them, $g_{ij} = |\mathbf{r}_j - \mathbf{r}_i|/d - 1$, goes to zero. This effect prevents the particle contact during the evolution. However, when a fixed time step is used in the numerical integration of the equations of motion, the particles may

overlap. It is important to realize that it is a pure numerical artifact of the integrating routine. This problem was already noted in the literature and was dealt with in variety of ways. One of the possibilities is to introduce a short-ranged repulsive potential to prevent the overlaps (see eg. [7, 9, 11–13]). A number of different potentials has been considered (e.g. inverse Hookean springs, power law etc.). Interestingly, in some cases the form and magnitude of the potential was found to significantly influence both the transport properties and the particle distribution function in the system [12, 13, 19]. Alternatively, in [20] the particles were allowed to overlap for a short period of time. However, the mobility matrix $\boldsymbol{\mu}$ is not defined for overlapping particles. To circumvent that difficulty, the authors of [20] for the sake of calculating mobility functions were shifting the overlapping particles apart so that they were separated by a non-dimensional gap of 10^{-8}.

Yet another method was used by Ladd [8]: reflect the particles elastically each time they are going to overlap. To be more precise, after calculating the particle velocities according to Eq. (4), the hard sphere dynamics is implemented over one time step: the possible collisions between the particles are located and then carried out, as described by Alder and Wainwright [21]. After the completion of the time step, δt, the hydrodynamic mobility matrix μ is calculated again, for the new particle positions ($\mathbf{X}(t+\delta t)$), and then the procedure is repeated.

The overlap problem may be avoided by decreasing the timestep as the spheres approach each other. One of such schemes was proposed by Ball and Melrose [10]: given the set of velocities calculated from (4), they detected the potential overlaps and decreased the time step in such a way as to prevent them.

In our numerical simulations we observed that the overlap may be avoided in an even more straightforward way by using the variable time-step Runge-Kutta method [22] as described in [16], for sufficiently high accuracy requirements (see also the discussion in Section V). However, no matter which variable time step method is used, there is a price to pay: although the particles no longer overlap, because of the presence of singular forces the close encounters of the particles involve very small timesteps and hence a considerable amount of computer time. This is undesirable when simulating many-particle systems, such as concentrated colloidal suspensions in which close encounters of the particles occur frequently. In this context, it is worth to explore in more detail alternative ways of preventing particle overlaps in order to find a method which would be both acceptably fast and accurate. To assess

the accuracy and effectiveness of the methods there is a a need for benchmark test system. Below, we propose such a benchmark trajectory, which involves three particles which remain constantly in close contact. A precise determination of the particle evolution along this trajectory constitutes a stringent test for the numerical methods, since the potential artifacts introduced by numerical treatment of overlaps in this case will become amplified in the course of time.

IV. PERIODIC MOTIONS OF VERY CLOSE SPHERES

In a number of systems, gravitational settling of a group of spheres has been detected experimentally [23] or evaluated by the Stokesian dynamics [24, 25], and a generic 'scattering' pattern of evolution has been found: initially well-separated particles approach each other, interact for some time, and separate again. The evolution can be very sensitive to a small change of the initial conditions [25]. Such a scenario sometimes involves very close configurations of the spheres, with the distance between the sphere surfaces smaller than 10^{-2} radii, for example when a sphere falls under gravity onto the other one held fixed or moving slower almost exactly below. [14, 15]. The particles stay close to each other, but for a short time only, and later on the interparticle distances grow indefinitely.

To test Stokesian dynamics at small separations between the particle surfaces, solutions of a different nature are needed: with a small number of non-touching spheres, which would move with respect to each other but stay very close for a long time. (Two identical spheres settle with no change of the relative configuration, therefore the simplest benchmark consists of three identical spheres.) Moreover, the particles should not change significantly their evolution under a small perturbation of the configuration. Therefore an ideal benchmark would be a periodic trajectory of close spheres.

Periodic oscillations of three settling particles are known from the literature, but for well-separated surfaces. The first experimental evidence [23] and theoretical derivation within the point-particle approximation [24] were followed by extended mathematical analysis of periodic solutions for points [26] and by investigation of periodic solutions for spherical particles [27].

In this work, we have found and analyzed periodic motion of three identical spheres settling under gravitational forces $\mathbf{f}$, with at least two very small gaps between their surfaces

at a time. Actually, we have found a class of quasi-periodic solutions with two incommensurate frequencies of oscillations. They surround a single-frequency solution, which will now be presented.

The z axis is chosen antiparallel to the gravitational force $\mathbf{f} = (0, 0, -f)$, with $f > 0$. The motion is restricted to a vertical plane y=0. Positions of the sphere centers are denoted as $\mathbf{r}_i = (x_i, 0, z_i)$, $i = 1, 2, 3$, and positions and velocities of the center of mass as $\mathbf{r}_{CM} = (x_{CM}, 0, z_{CM})$ and $\mathbf{v}_{CM} = (v_{x,CM}, 0, v_{z,CM})$, respectively.

The initial positions of the sphere centers, corresponding to the single frequency solution, are

$$x_1 = -x_3 \approx 0.626266,\ z_1 = -z_3 \approx -0.779612 \text{ and } \ x_2 = z_2 = 0. \tag{8}$$

Therefore initially the sphere centers are aligned, with two equal interparticle distances, $r_{12} = r_{23}$, where $r_{ij} = |\mathbf{r}_{ij}|$ and $\mathbf{r}_{ij} = \mathbf{r}_i - \mathbf{r}_j$, corresponding to narrow gaps $r_{12} - 1 \approx 2 \times 10^{-6}$ between the sphere surfaces. This configuration is shown in the first frame of Fig. 1.

The solution of the dynamics given by Eqs. (3), (4) and (8) is a superposition of a periodic motion with the period $T \approx 170$, and the gravitational settling with the time-averaged velocity

$$\mathbf{V} = \frac{1}{T} \int_0^T \mathbf{v}_{CM}\, dt \approx -1.85\, \mathbf{e}_z. \tag{9}$$

Evolution of the system is illustrated in Fig. 1, as seen by an observer moving vertically with the time-averaged velocity $\mathbf{V}$, and taking snapshots at the subsequent time instants separated by $T/36$. Two characteristic symmetric configurations of the spheres are observed. In the first one, seen at $t = 0$ and then every $T/6$, the centers are aligned at the angle $\theta \approx 39^\circ$ with respect to gravity, with the equal sizes of both gaps between the particle surfaces. In the second configuration, which appears at $t = T/12$ and later after each $T/6$, the sphere centers form an isosceles triangle with a vertical base, not much different from the equilateral one. The generic pattern of the evolution during $T/6$, depicted in Fig. 1, is then repeated, with the corresponding interchange of the particles, and the left-right symmetry between the configurations at t and $t + T/6$.

As shown in Fig. 1, the center-of-mass oscillates while settling, with the dominant horizontal component. The horizontal velocity is the largest for the first and the last snapshots of Fig. 1, i.e. for the aligned particles, see also Fig. 2. In this case, the sideways motion can be understood by analogy with two settling spheres or an oblique rod [28, 29].

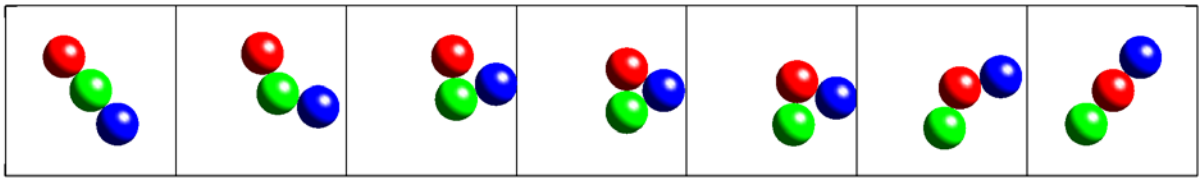

FIG. 1: Configurations of the sphere centers at $t = T(n-1)/36$, with $n = 1, 2, ..., 7$, as seen by an observer settling vertically with the time-averaged velocity $\mathbf{V}$.

The explicit time-dependence of $\mathbf{v}_{CM}$ is shown in Fig. 2, where the horizontal and vertical components of the center-of-mass velocity are plotted as functions of time, in the frame settling vertically with the time-averaged velocity $\mathbf{V}$. Note that the center-of-mass motion is characterized by the period equal to $T/3$ rather than T. The time-dependence of $v_{z,CM}$

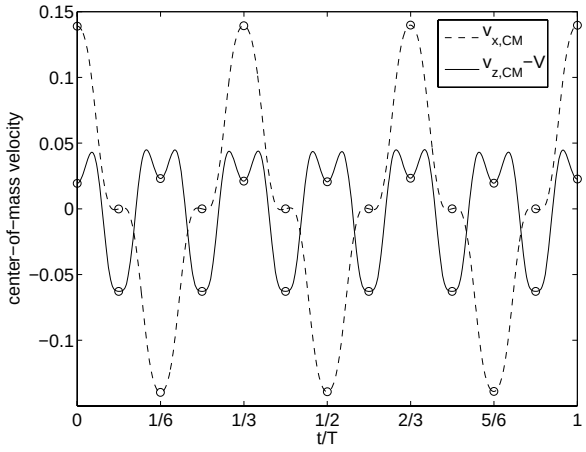

FIG. 2: The instantaneous center-of-mass velocity as measured by an observer settling with the time-averaged velocity V. The symbols $\circ$ denote the positions at every $T/12$.

indicate that vertical settling is the fastest for the almost equilateral configuration of the sphere centers seen at the middle snapshot of Fig. 1, i.e. at $t = T/12$, and then after every $T/6$. On the other hand, settling is the slowest for the configurations seen at the second and the last but one snapshot, at $t = T/36$ and $t = 5T/36$, and then every $T/6$ after these time instants. Such a configuration corresponds also to the minimum of the inter-particle distances, as shown in Fig. 3. The minimal gap size is reached for only one pair of the spheres at a time and it is as small as 3.5×10^{-8}. Therefore, the logarithmic scale is used in Fig. 3 while plotting the distance between the sphere surfaces $r_{ij} - 1$ versus time.

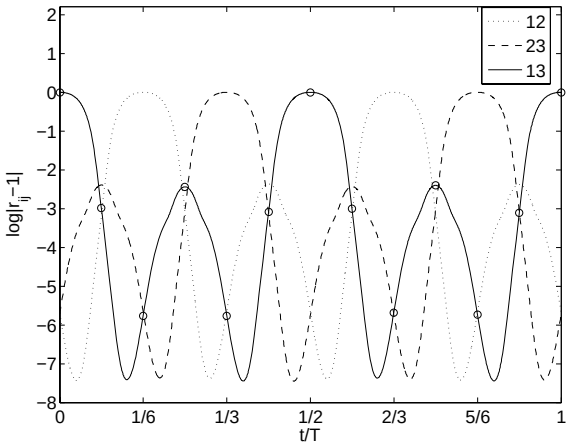

FIG. 3: The logarithm of the distance between the sphere surfaces. The symbols ∘ denote values of $\log(r_{13}-1)$ at every $T/12$.

Trajectories of the centers of the spheres $z_i(x_i)$ and of the center of mass $z_{CM}(x_{CM})$ during a single period T are plotted in Fig. 4.

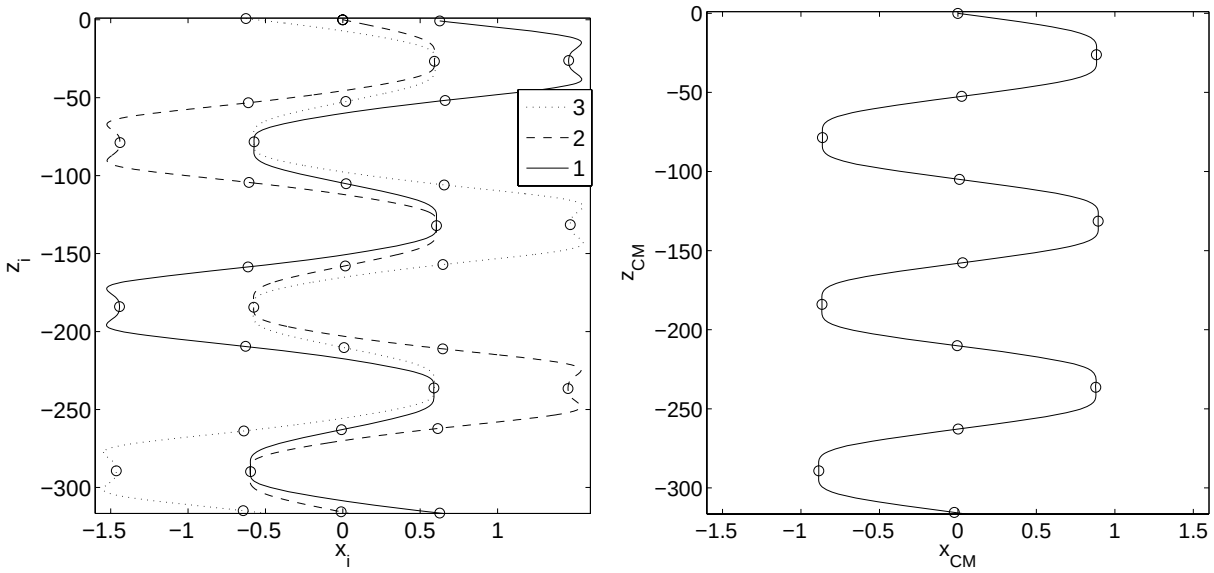

FIG. 4: Trajectories of the sphere centers (left) and of their center of mass (right), in the lab frame. One period $T \approx 170$ is shown. The symbols ∘ denote the positions at every $T/12$.

It is worthwhile to subtract the settling motion and obtain closed trajectories of the sphere centers. One possibility is to adopt the center-of-mass frame. The corresponding trajectories, $z_i - z_{CM}$ versus $x_i - x_{CM}$, are plotted in Fig. 5, with the corresponding movie linked on line. A striking feature is that we obtain as the result a single closed trajectory

for all the three spheres. The particles circle along the same orbit, with the $T/3$ shift with respect to each other. The "butterfly" shape of this trajectory is also of a special interest because of the existence of cusps – points, where the motion rapidly changes direction.

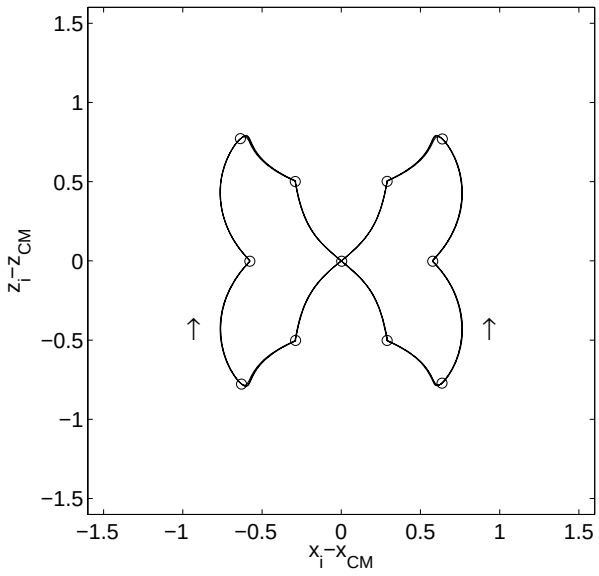

FIG. 5: The unique "butterfly" trajectory of all the sphere centers, in the center-of- mass frame. The sense of the motion is indicated by the arrows. The symbols ∘ denote the positions at every $T/12$ (enhanced on line).

An alternative description of the relative motion is to use the relative coordinates of the sphere centers, $(x_{ij}, 0, z_{ij}) = \mathbf{r}_{ij}$. The resulting trajectory, $z_{23}(x_{23})$, identical to $-z_{13}(x_{13})$, is plotted in Fig. 6. Surprisingly, this curve contains tips – the turning points, where the direction of the relative motion is reversed. The motion of the sphere centers with respect to the center of sphere 3 is shown in the movie linked on line. This movie illustrates that, most of the time, the shearing motion of the surfaces dominates the squeezing one. In Fig. 7, both squeezing v_n and shearing v_t components of the relative velocity $\mathbf{v}_{23}$ are plotted versus time. Indeed, the squeezing component v_n is practically negligible most of the time. Moreover, rapid changes of v_n from/to zero correspond to significant changes of the direction of the relative motion, observed at the cusps and tips of the relative trajectory in Fig. 6.

With three dimensional numerical codes, we did not observe separation of the particles nor a change of the periodic benchmark solution even after 100 periods. The periodic solution presented above is robust, although it slowly moves out of the vertical plane and eventually the particles separate, if an off- plane perturbation is applied. On the other

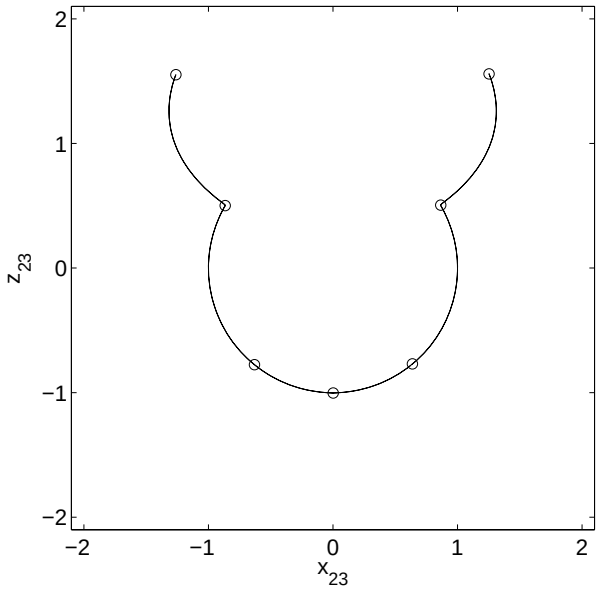

FIG. 6: The relative trajectory of the sphere centers. The positions are denoted by ∘ at every $T/12$ (enhanced on line).

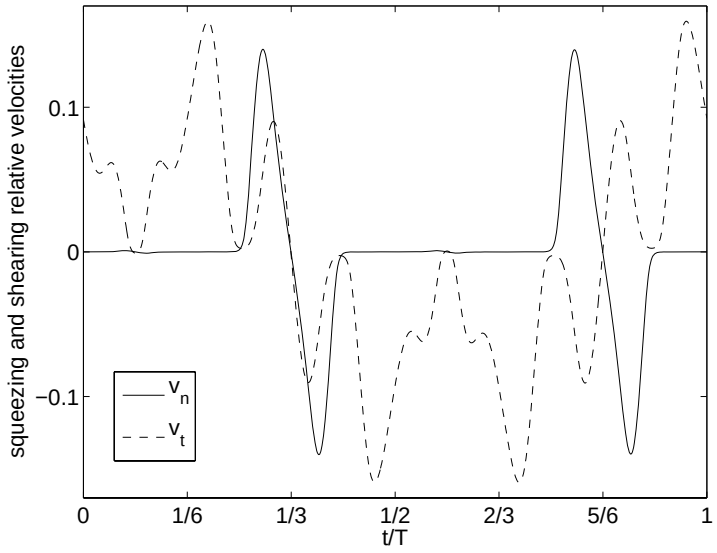

FIG. 7: Evolution of the squeezing and shearing components of the relative velocity, $v_n = \mathbf{v}_{23} \cdot \hat{\mathbf{n}}$ and $v_t = \mathbf{v}_{23} \cdot \hat{\mathbf{t}}$, with $\hat{\mathbf{n}} = \mathbf{r}_{23}/r_{23} = (\sin\theta, 0, \cos\theta)$ and $\hat{\mathbf{t}} = (\cos\theta, 0, -\sin\theta)$.

hand, if the "optimal" initial conditions (8) are slightly perturbed within the plane, the particles still oscillate, but quasi-periodically, with a second additional frequency. Such a behavior is generic even for such a symmetric initial configuration of the particle centers as

the equilateral triangle with a vertical base. For example, for the size of its side equal to 1.01, the spectral density of $x_2(t)$ was computed and plotted in Fig. 8, side by side with the spectral density corresponding the the "optimal" solution. The frequency f_1 corresponds

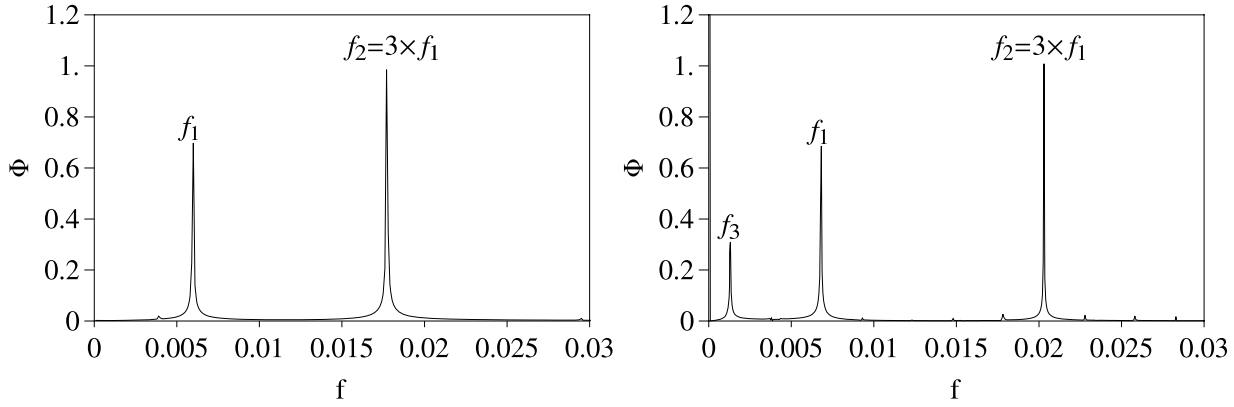

FIG. 8: Spectral density Φ (square of the magnitude of the Fourier transform) of $x_2(t)$, i.e. the horizontal coordinate of a particle as a function of time. Left: the optimal trajectory with initial conditions given by Eq. (8). Right: a slightly perturbed trajectory with respect to the optimal one. The spectral density $\Phi(f)$ was normalized to one at the maximum.

to the period of oscillations of the relative motion ($T \approx 170$ for the optimal trajectory), whereas the frequency $f_2 = 3f_1$ corresponds to the oscillations of the center of mass of the system (*cf.* Fig. 1). Finally, a smaller peak (f_3) on the right panel corresponds to the slow modulation around the periodic orbit. This modulation is inherent to the motion of the center of mass. For the solutions analyzed in Fig. 8, the corresponding plots of the spectral density of $x_2 - x_{CM}$ contain only the single peak f_1, and the plot of the spectral density of x_{CM} – only peaks f_2 and f_3 for the perturbed trajectory. Note that the positions of the peaks on both panels do not coincide, which shows that the period of the motion changes as the trajectory is perturbed.

V. TESTING INTEGRATION SCHEMES

In this section we analyze influence of integration routine and the method of avoiding overlaps on the sphere dynamics. We test three different algorithms to integrate Eqs. (5)-(6). In each of them we apply the same procedure to evaluate the mobility matrix, following Sec. II. As mentioned in Sec. III, constant time-step methods can lead to non-physical

overlapping of spheres. Adaptive routines can avoid that problem, but they are slow, because as the spheres approach each other, the time step is decreased to very small values. Testing the accuracy of fixed time-step procedures, we will use the fourth order Runge- Kutta with adaptive time-step (RK) and the error density per unit time $\rho = 10^{-10}$ (for the definition see Appendix A) as the benchmark routine. In RK method, the overlaps are avoided by an additional decreasing of the time-step by the factor of two if a potential overlap is detected. However, it turns out that for $\rho \leq 10^{-6}$, even the standard adaptive RK procedure does not lead to the overlaps and the additional time- step reduction is not needed.

As the method of avoiding overlaps in the fixed time-step methods we apply elastic collision method, described in Ref. [8] and outlined in Section III. Collisions are incorporated into two integration schemes: fourth order Runge- Kutta method and implicit Euler technique (described in Appendix B). Summarizing, we compare results of three different integrating algorithms: adaptive fourth order Runge-Kutta (RK), constant time step fourth order Runge-Kutta with collisions (RKC) and implicit Euler with collisions (IEC).

As a benchmark problem for assessing the accuracy and the efficiency of various numerical schemes, we use the periodic motion of three spheres described in the previous section. This gives a possibility to monitor such characteristics as the period or the minimal distance between the sphere surfaces on the trajectory, depending on the method.

Using less accurate routines is reasonable if they are faster then our reference method. To measure routine efficiency we will use T_{CPU}, which is the time (in seconds) that CPU needs to calculate the system evolution during the time unit τ_s, defined in Eq. (7). For constant time-step routines, T_{CPU} is almost constant during evolution. In adaptive Runge-Kutta method time step is decreasing when spheres are closer to each other, so T_{CPU} should increase in such cases. Indeed, such a tendency can be observed in Fig. 9, where we plot T_{CPU} and the minimal distance between all the three pairs of spheres,

$$\xi = \min(r_{12}, r_{23}, r_{31}) - 1. \tag{10}$$

The results obtained with different integration schemes are compared in Fig. 10 and Table I. For the fixed time-step routines, three values of the time step are used to control the convergence. For RK procedure the time-step is changing, but we can control average time-step $< dt >$ by changing error density per unit time ρ. For the data in Fig. 10 and Table I we choose ρ in such a way as to obtain $< dt >$ similar to the values used in the fixed

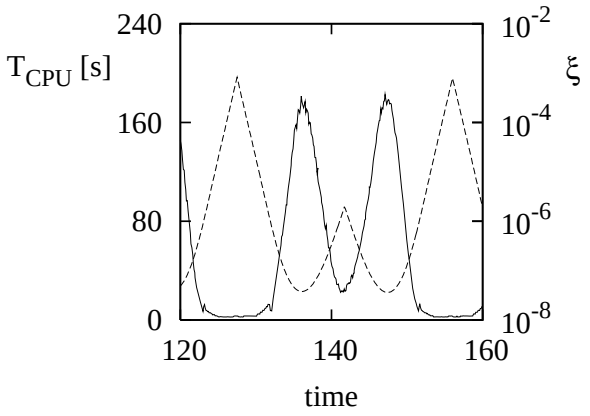

FIG. 9: Computational time of the adaptive RK method T_{CPU} (solid line) and the corresponding minimal distance ξ given by Eq. (10) (dashed line) as a function of time. Initial positions of all the three spheres are given by Eq. (8) and the error density per unit time $\rho = 10^{-9}$.

time-step routines. In Fig. 10 the logarithm of the distance between surfaces of one pair of spheres is shown as a function of time, whereas in Table I also other features of the periodic trajectory are explicitly compared: period T, minimal distance r_{min} between the surfaces on the trajectory and the average computational time $< T_{CPU} >$.

	time-step	period T	minimal distance r_{min}	$\langle T_{CPU} \rangle$ [s]
	$dt = 0.1$	151	$3 \cdot 10^{-10}$	3.2
IEC	$dt = 0.01$	186	$1.1 \cdot 10^{-12}$	5.2
	$dt = 0.001$	209	$5 \cdot 10^{-15}$	60.4
	$dt = 0.1$	129	10^{-5}	0.9
RKC	$dt = 0.01$	153	$2 \cdot 10^{-7}$	9.2
	$dt = 0.001$	170	$3.5 \cdot 10^{-8}$	170
RK $\rho = 10^{-1}$	$\langle dt \rangle \approx 0.081$	147	$3.3 \cdot 10^{-7}$	1.2
$\rho = 10^{-6}$	$\langle dt \rangle \approx 0.009$	171	$2.7 \cdot 10^{-8}$	15
$\rho = 10^{-10}$	$\langle dt \rangle \approx 0.001$	170	$3.7 \cdot 10^{-8}$	110

TABLE I: Comparison of three different integration schemes (IEC, RKC, RK), applied to the same initial condition given by Eq. (8). Basic features of the calculated periodic trajectories (period and minimal distance) and average efficiency of the numerical computation $\langle T_{CPU} \rangle$.

.

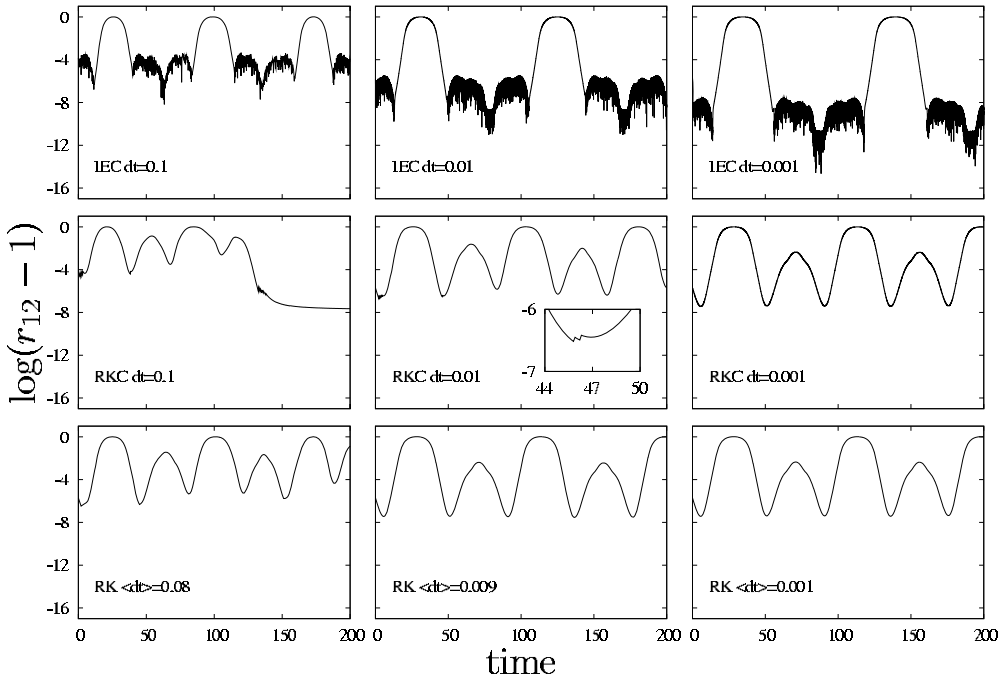

FIG. 10: The distance between surfaces of two spheres, labeled 1 and 2, as a function of time, obtained with the use of three methods: IEC, RKC and RK. The corresponding time-steps (or average time-step for RK) are indicated in panels. The initial positions of all the spheres are given by Eq. (8).

A striking feature of Fig. 10 is the presence of long chains of collisions, corresponding to non-smooth parts of the plots. This shows, surprisingly, that single collisions are rare. The effect of collisions is the most significant in the IEC procedure; actually, the collisions change the dynamics of very close particles in a profound way. In case of the implicit Euler scheme, paradoxically, the collisions induce the tendency of particles to stay together longer and at smaller distances that the ones calculated by the reference fourth order adaptive RK scheme [31]. Decreasing the time-step in IEC procedure, we observe that period of the motion is constantly increasing whereas minimal distance between the spheres surfaces is decreasing, reaching the numerical noise level at $dt = 0.001$. Therefore IEC routine does not seem to converge. Moreover, the results of IEC method differ from those obtained with the RK routine. For the IEC scheme with the smallest time-step $dt = 0.001$ the period is $T = 209$ and the minimal distance between the sphere surfaces $r_{min} = 5 \cdot 10^{-15}$. For the reference RK with the average $< dt >= 0.001$, the period and the minimal distance between

the sphere surfaces are $T = 170$ and $r_{min} = 3 \cdot 10^{-8}$, respectively.

Contrary to the IEC, the RKC routine does converge. Decreasing the time-step in RKC, we reproduce the reference result of the RK integration scheme, as indicated in Fig. 10 and Table I. Such result is to be expected, because for $dt \leq 0.001$ there are no collisions. However, for such small dt, the computational time T_{CPU} increases considerably, and it becomes even larger than for adaptive RK. If we use larger time-steps in RKC, there is some gain in T_{CPU}, but the period and minimal distance change significantly.

VI. CONCLUSIONS

In this study, we considered the dynamics of close spherical particles moving in a viscous fluid. A benchmark periodic trajectory of three spheres was found, with the particles remaining constantly within a very short distance to each other. The period of the motion corresponds to about 170 τ_s (85 Stokes times), and the longest simulations reported reached more than 100 periods. Most of the time the particles are in sliding motion relative to each other, followed by rapid changes of direction of the relative motion. The smallest gap between the particles constantly remains below 1% of their diameter. This is in contrast to previously reported trajectories which have mostly a scattering character, i.e. after some interaction time initially close particles drift away from each other. Constant proximity of the particles makes the considered trajectory an ideal benchmark problem for a comparison of accuracy between different numerical methods. In particular, it is then possible to test different approaches of solving the problem of particle overlaps, which are a non-physical, numerical artifact of most fixed time-step integrating routines. The results of our analysis show that the details of the particle motion strongly depend on both numerical method used to integrate the equations of motion and the adopted method of avoiding the overlaps. In particular, we show that the elastic collision method (in which the particles are reflected elastically each time they are going to overlap) inevitably introduces significant errors, which are hard to control, unless the timestep is sufficiently reduced so that the collisions are rare. The adaptive time step routines, although slower in terms of computational speed, are in general much more accurate than collision methods and thus appear to be the method of choice for the Stokesian dynamics simulations of close particles.

Acknowledgments

The numerical code used in this work was based on the routines for calculation of hydrodynamic matrices written by E. Wajnryb and the hard-sphere dynamics routine by A.J.C. Ladd. The movies were created with VMD [30]. M. L. E.-J. benefited from the COST Action P21 "Physics of Droplets". The work of M. L. E.-J. and T. G. was supported in part by the Polish Ministry of Science and Higher Education Grant No. COST/116/2007.

APPENDIX A: ERROR CALCULATION IN ADAPTIVE RUNGE-KUTTA METHOD

In this Appendix, we discuss the accuracy of the adaptive Runge-Kutta algorithm, following [22]. A good estimate of a truncation error of the algorithm is

$$\Delta_1(dt) = \sqrt{\sum_{i=1}^{3} |\mathbf{r}_i^{(5)}(t+dt) - \mathbf{r}_i^{(4)}(t+dt)|^2}, \tag{A1}$$

where $|\mathbf{r}_i^{(5)}(t+dt) - \mathbf{r}_i^{(4)}(t+dt)|$ is the difference between fifth order and fourth order Runge-Kutta results for the position of particle i at the next timestep, dt. This error is then compared with the desired accuracy, Δ_0:

$$\Delta_0(dt) = \rho dt, \tag{A2}$$

where ρ is the error density per unit time, specified at the beginning of the simulation. A new value of the timestep, dt', is then calculated as [22]:

$$dt' = \begin{cases} Sdt \left|\frac{\Delta_0}{\Delta_1}\right|^{1/5} & \text{if } \Delta_0 \geq \Delta_1, \\ Sdt \left|\frac{\Delta_0}{\Delta_1}\right|^{1/4} & \text{if } \Delta_0 < \Delta_1, \end{cases} \tag{A3}$$

where we take the safety factor S equal to 0.95.

APPENDIX B: IMPLICIT AND EXPLICIT EULER METHOD WITH COLLISIONS

As described in III, the explicit Euler method with hard-sphere collisions may be represented formally as

$$\mathbf{X}(t+\delta t) = \mathbf{X}(t) + [\mathbf{V}(\mathbf{X}(t))\delta t]_{HS} \tag{B1}$$

where an index HS means that a hard sphere dynamics is used to advance the system by δt. In the above equation the particle velocities are computed at the beginning of the time step, just as in any explicit (forward) Euler method. However, explicit Euler method suffers from numerical instability problem and one needs to resort to impractically short time steps to obtain reliable results. To avoid this problem, a following implicit scheme may be used

$$\mathbf{X}(t+\delta t) = \mathbf{X}(t) + [\mathbf{V}(\mathbf{X}(t+\delta t))\delta t]_{HS} \tag{B2}$$

which we are going to call "implicit Euler method with collisions" (IE). A downside of this method is that $\mathbf{X}(t+\delta t)$ is given only implicitly by the above equation. To find $\mathbf{X}(t+\delta t)$, we use a fixed point iteration scheme, with an initial guess $\mathbf{X}^0(t+\delta t) = \mathbf{X}(t)$. The iterations are stopped when the difference between the values of $\mathbf{X}(t+\delta t)$ calculated in successive iterations is smaller than 10^{-5}.

---

[1] S. Kim and S. J. Karrila, *Microhydrodynamics: Principles and Selected Applications* (Butterworth-Heinemann, London, 1991).

[2] J. Happel and H. Brenner, *Low Reynolds Number Hydrodynamics* (Noordhoff, Leyden, 1973).

[3] A. J. C. Ladd, "Numerical simulations of particulate suspensions via a discretized Boltzmann equation," J. Fluid Mech. **271**, 285–339 (1994).

[4] J. F. Brady and G. Bossis, "Stokesian dynamics," Ann. Rev. Fluid Mech. **20**, 111–157 (1988).

[5] B. Cichocki, B. U. Felderhof, K. Hinsen, E. Wajnryb, and J. Bławzdziewicz, "Friction and mobility of many spheres in Stokes flow," J. Chem. Phys. **100**, 3780–3790 (1994).

[6] D. J. Jeffrey and Y. Onishi, "The Forces and Couples Acting on Two Nearly Touching Spheres in Low-Reynolds-Number Flow," Z. Ang. Math. Phys. **35**, 634–641 (1984).

[7] G. Bossis and J. F. Brady, "Dynamic simulation of sheared suspensions. I. General method," J. Chem. Phys. **80**, 5141–5154 (1984).

[8] A. J. C. Ladd, "Dynamical simulations of sedimenting spheres," Physics of Fluids **5**, 299–310 (1993).

[9] A. Sierou and J. F. Brady, "Shear-induced self-diffusion in non-colloidal suspensions," Journal of Fluid Mechanics **506**, 285–314 (2004).

[10] R. C. Ball and J. R. Melrose, "Lubrication breakdown in hydrodynamic simulations of concentrated colloids," Advances in Colloidal Interface Science **59**, 19–30 (1995).

[11] R. C. Ball and J. R. Melrose, "A simulation technique for many spheres in quasi-static motion under frame-invariant pair drag and Brownian forces," Physica A **247**, 444–472 (1997).

[12] S. L. Dance, E. Climent, and M. R. Maxey, "Collision barrier effects on the bulk flow in a random suspension," Physics of Fluids **16**, 828–831 (2004).

[13] D. I. Dratler, W. R. Schowalter, and R. L. Hoffman, "Dynamic simulation of shear thickening in concentrated colloidal suspensions," Journal of Fluid Mechanics **353**, 1–30 (1997).

[14] R. H. Davis, "Effects of surface roughness on a sphere sedimenting through a dilute suspension neutrally buoyant spheres," Phys. Fluids A **4**, 2607–2619 (1992).

[15] M. L. Ekiel-Jeżewska, F. Feuillebois, N. Lecoq, K. Masmoudi, R. Anthore, F. Bostel, and E. Wajnryb, "Hydrodynamic interactions between two spheres at contact," Phys. Rev. E **59**, 3182–3191 (1999).

[16] M. L. Ekiel-Jeżewska and E. Wajnryb, "Equilibria for the relative motion of three heavy spheres in Stokes fluid flow," Phys. Rev. E **73**, 046 309 (2006).

[17] B. Cichocki, M. L. Ekiel-Jeżewska, and E. Wajnryb, "Lubrication corrections for three-particle contribution to short-time self-diffusion coefficients in colloidal dispersions," J. Chem. Phys. **111**, 3265–3273 (1999).

[18] B. U. Felderhof, "Many-body hydrodynamic interactions in suspensions," Physica A **151**, 1–16 (1988).

[19] G. Drazer, J. Koplik, B. Khusid, and A. Acrivos, "Deterministic and stochastic behaviour of non-Brownian spheres in sheared suspensions," Journal of Fluid Mechanics **460**, 307–335 (2002).

[20] T. N. Phung, J. F. Brady, and G. Bossis, "Stokesian Dynamics simulation of Brownian suspensions," Journal of Fluid Mechanics **313**, 181–207 (1996).

[21] B. J. Alder and T. E. Wainwright, "Studies in Molecular Dynamics II. Behavior of a Small Number of Elastic Spheres," Journal of Chemical Physics **33**, 1439–1451 (1960).

[22] W. H. Press, B. P. Flannery, S. A. Teukolsky, and W. T. Vetterling, *Numerical Recipes: The Art of Scientific Computing* (Cambridge University Press, Cambridge (UK) and New York, 1992), 2nd edn.

[23] K. O. L. F. Jayaweera, B. J. Mason, and G. W. Slack, "The behaviour of clusters of spheres

falling in a viscous fluid. Part 1. Experiment," J. Fluid Mech. **20**, 121–128 (1964).

[24] L. M. Hocking, "The behaviour of clusters of spheres falling in a viscous fluid. Part 2. Slow motion theory," J. Fluid Mech. **20**, 129–139 (1964).

[25] I. M. Jánosi, T. Tél, D. E. Wolf, and J. A. C. Gallas, "Chaotic particle dynamics in viscous flows: The three-particle Stokeslet problem," Phys. Rev. E **56**, 2858–2868 (1997).

[26] M. Golubitsky, M. Krupa, and C. Lim, "Time-reversibility and particle sedimentation," SIAM J. Appl. Math. **51**, 49–72 (1991).

[27] R. E. Caflisch, C. Lim, J. H. C. Luke, and A. S. Sangani, "Periodic solutions for three sedimenting spheres," Phys. Fluids **31**, 3175–3179 (1988).

[28] E. J. Hinch, "Sedimentation of small particles," in *Disorder and Mixing*, E. Guyon, J.-P. Nadal, and Y. Pomeau, eds. (Kluwer, Dordrecht, 1988), pp. 153–161.

[29] G. I. Taylor, *Low Reynolds number flow* (The National Committee for Fluid Mechanics Films Chicago: Encyclopaedia Britannica Educational Corporation, Chicago, 1967).

[30] W. Humphrey, A. Dalke, and K. Schulten, "VMD – Visual Molecular Dynamics," Journal of Molecular Graphics **14**, 33–38 (1996).

[31] The unphysical tendency of the IEC procedure to 'glue' the particles together actually helped us to find the family of 'butterfly' periodic and quasi-periodic trajectories.